CHEMISTRY
A EUROPEAN JOURNAL

DOI: 10.1002/chem.200800585

1,4-Dicyanobenzene as a Scaffold for the Preparation of Bimetallic Actinide Complexes Exhibiting Metal–Metal Communication

Eric J. Schelter, Jacqueline M. Veauthier, Christopher R. Graves, Kevin D. John, Brian L. Scott, Joe D. Thompson, Jaime A. Pool-Davis-Tournear, David E. Morris,* and Jaqueline L. Kiplinger*[a]

Abstract: Reaction of two equivalents of $[(C_5Me_4Et)_2U(CH_3)(Cl)]$ (**6**) or $[(C_5Me_5)_2Th(CH_3)(Br)]$ (**7**) with 1,4-dicyanobenzene leads to the formation of the novel 1,4-phenylenediketimide-bridged bimetallic organoactinide complexes $[\{(C_5Me_4Et)_2(Cl)U\}_2(\mu\text{-}\{N{=}C(CH_3)\text{-}C_6H_4\text{-}(CH_3)C{=}N\})]$ (**8**) and $[\{(C_5Me_5)_2(Br)Th\}_2(\mu\text{-}\{N{=}C(CH_3)\text{-}C_6H_4\text{-}(CH_3)C{=}N\})]$ (**9**), respectively. These complexes were structurally characterized by single-crystal X-ray diffraction and NMR spectroscopy. Metal–metal interactions in these isovalent bimetallic systems were assessed by means of cyclic voltammetry, UV-visible/NIR absorption spectroscopy, and variable-temperature magnetic susceptibility. Although evidence for magnetic coupling between metal centers in the bimetallic U^{IV}/U^{IV} ($5f^2$–$5f^2$) complex is ambiguous, the complex displays appreciable electronic communication between the metal centers through the π system of the dianionic diketimide bridging ligand, as judged by voltammetry. The transition intensities of the f–f bands for the bimetallic U^{IV}/U^{IV} system decrease substantially compared to the related monometallic ketimide chloride complex, $[(C_5Me_5)_2U(Cl)\{\text{-}N{=}C(CH_3)\text{-}(3,4,5\text{-}F_3\text{-}C_6H_2)\}]$ (**11**). Also reported herein are new synthetic routes to the actinide starting materials $[(C_5Me_4Et)_2U(CH_3)(Cl)]$ (**6**) and $[(C_5Me_5)_2Th(CH_3)(Br)]$ (**7**) in addition to the syntheses and structures of the monometallic uranium complexes $[(C_5Me_4Et)_2UCl_2]$ (**3**), $[(C_5Me_4Et)_2U(CH_3)_2]$ (**4**), $[(C_5Me_4Et)_2U\{\text{-}N{=}C(CH_3)\text{-}C_6H_4\text{-}C{=}N\}_2]$ (**10**), and **11**.

Keywords: actinides · bimetallic complexes · electrochemistry · electronic communication · magnetic properties

Introduction

The rich magnetic and electrochemical properties of the 5f elements make actinide-based functional materials an intriguing prospect.[1] However, exploiting these properties requires a fundamental understanding of how to promote and control short-range electronic delocalization and magnetic exchange interactions between actinide metal centers; mastery that has been attained for transition metals, but not for the actinides.[1e,f,2] To date, much attention has been paid to the synthesis of high nuclearity polyoxo clusters; however, the actinide–actinide interactions in these systems have been too weak for any clear detection.[3] In contrast to transition metals, self-assembled actinide frameworks that are held together by noncovalent bonds also exhibit little to no metal–metal interaction.[4]

Although a few examples of magnetic exchange between 5f and 3d metals have been reported,[5] the only approach that has been successful in promoting interactions between actinide ions in molecular complexes has been through the use of covalently linked bridging ligands. For example, imido linkages were employed in the single example of unambiguous $5f^1$–$5f^1$ antiferromagnetic coupling in $[\{(Me\text{-}C_5H_4)_3U^V\}_2(\mu\text{-}1,4\text{-}N_2C_6H_4)]$ (**1**).[6] Furthermore, use of ketimide ligand linkages allowed clear actinide-mediated electronic delocalization in $[(C_5Me_5)_2U^{IV}(\text{-}N{=}C(Bz)\{tpy\text{-}U^{III}\text{-}(C_5Me_4Et)_2\})_2]$ (**2**).[7] Although appreciable $5f^3$-$5f^2$-$5f^3$ magnetic interactions were also anticipated for **2**—derived from direct exchange by overlap with local SOMOs on the intervening reduced terpyridyl groups—the ligand field signatures of the uranium ions in the χT product for this complex masked any signatures for magnetic interactions.

[a] Dr. E. J. Schelter, Dr. J. M. Veauthier, Dr. C. R. Graves, Dr. K. D. John, Dr. B. L. Scott, Dr. J. D. Thompson, Dr. J. A. Pool-Davis-Tournear, Dr. D. E. Morris, Dr. J. L. Kiplinger
Los Alamos National Laboratory
Mail Stop J514, Los Alamos, NM 87545 (USA)
Fax: (+1) 505-667-9905
E-mail: kiplinger@lanl.gov

Supporting information for this article is available on the WWW under http://dx.doi.org/10.1002/chem.200800585.

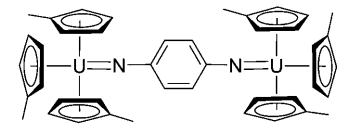

1

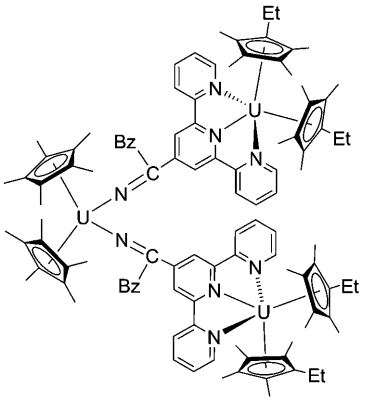

2

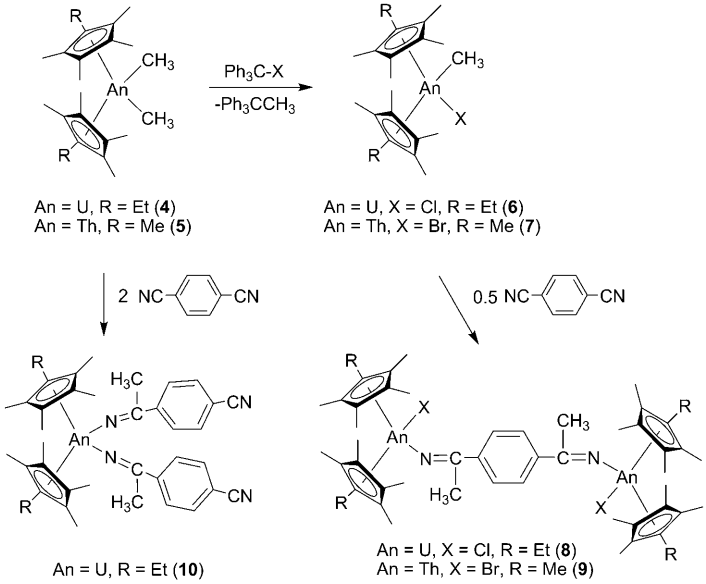

Scheme 1. Synthetic outline for the preparation of complexes **6**–**10**.

The nitrile insertion chemistry that has been successfully applied by our group in the synthesis of monometallic uranium and thorium ketimide complexes, as well as **2**, represents a rational synthetic strategy for crafting well-defined bimetallic actinide complexes.[8] The use of an aromatic spacer equipped with two ketimide functional groups as the covalent anchors for the actinide–actinide framework should allow manipulation of the metal combinations and the properties (substitution pattern, type of π network) of the bridging ligands to tune the electronic and magnetic interactions between the metal centers. Within such a covalent diketimide ligand framework, the study of a superexchange mechanism between the two uranium ions could be facilitated, which was previously effective for observation of magnetic exchange in **1**.

Herein, we report that nitrile insertion chemistry with 1,4-dicyanobenzene can be used to prepare 1,4-phenylenediketimide-bridged bimetallic thorium ($5f^0$–$5f^0$) and uranium ($5f^2$–$5f^2$) complexes, and that the uranium system displays clear signatures of electronic communication between the two metal centers through the π system of the novel dianionic bridging ligand. In the course of these studies we developed synthetic routes to $(C_5Me_4Et)MgCl{\cdot}THF$ and several monometallic thorium and uranium complexes, which we also describe.

Results and Discussion

Synthesis of bimetallic actinide complexes 8 and 9: Entry into this new class of bimetallic organoactinide compounds is illustrated in Scheme 1. The uranium system required the synthesis of $[(C_5Me_4Et)_2UCl_2]$ (**3**) and $[(C_5Me_4Et)_2U(CH_3)_2]$ (**4**), which were prepared in an analogous fashion to the known C_5Me_5 derivatives.[9] Namely, reaction of $(C_5Me_4Et)MgCl{\cdot}THF$ (2.2 equiv) with UCl_4 in toluene gave $[(C_5Me_4Et)_2UCl_2]$ (**3**) as a dark red crystalline solid in 97% isolated yield. Subsequent treatment of **3** with excess MeMgBr in Et_2O/dioxane gave dark red **4** in 72% yield following workup. Complexes **3** and **4** have been structurally characterized. As shown in Figure 1, the molecular structures of **3** and **4** reveal a bent metallocene framework with a pseudotetrahedral coordination environment about the uranium metal centers and the two chloride (U(1)–Cl(1) = 2.591(4) Å, U(1)–Cl(2) = 2.598(4) Å) or methyl (U(1)–C(23) = 2.429(4) Å, U(1)–C(24) = 2.415(4) Å) ligands, respectively, residing within the metallocene wedge. The metrical parameters in these complexes are as expected and compare well to other structurally characterized uranium(IV) chloride[10] and methyl[8a] complexes.

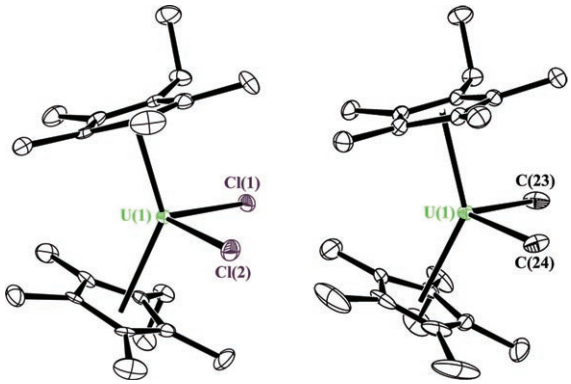

Figure 1. Molecular structures of complexes **3** (left) and **4** (right) with thermal ellipsoids at the 50% probability level. Hydrogen atoms are omitted for clarity. Selected bond lengths [Å] and angles [°] for **3**: U(1)–Cl(1) 2.591(4), U(1)–Cl(2) 2.598(4), Cl(1)–U(1)–Cl(2) 97.19(13), U(1)–$C_5Me_4Et_{(cent)}$ 2.44(1), $C_5Me_4Et_{(cent)}$–U(1)–$C_5Me_4Et_{(cent)}$ 137.4(3). Selected bond lengths [Å] and angles [°] for **4**: U(1)–C(23) 2.429(4), U(1)–C(24) 2.415(4), C(23)–U(1)–C(24) 95.22(15), U(1)–$C_5Me_4Et_{(cent)}$ 2.454(4), 2.459(4), $C_5Me_4Et_{(cent)}$–U(1)–$C_5Me_4Et_{(cent)}$ 141.0(1).

The mixed methyl chloride complex $[(C_5Me_4Et)_2U(CH_3)(Cl)]$ (**6**) was nearly quantitatively prepared in situ by treating a solution of **4** in toluene with the methide-abstracting agent, Ph_3CCl.[11] Although **6** was not isolated, it was characterized by ^1H NMR spectroscopy. Subsequent addition of 1,4-dicyanobenzene (0.5 equiv) to **6** yielded brown crystalline $[\{(C_5Me_4Et)_2(Cl)U\}_2(\mu\text{-}\{N{=}C(CH_3)\text{-}C_6H_4\text{-}(CH_3)C{=}N\})]$ (**8**) in 43% isolated yield. The moderate yield reflects the high solubility of complex **8**. The bimetallic thorium analogue $[\{(C_5Me_5)_2(Br)Th\}_2(\mu\text{-}\{N{=}C(CH_3)\text{-}C_6H_4\text{-}(CH_3)C{=}N\})]$ (**9**) was made in a similar fashion and obtained as an orange crystalline solid in 14% yield from 1,4-dicyanobenzene (0.5 equiv) and $[(C_5Me_5)_2Th(CH_3)(Br)]$ (**7**), which was generated from $[(C_5Me_5)_2Th(CH_3)_2]$ (**5**) and Ph_3CBr.

The C_5Me_4Et ligand framework was chosen for crystallinity reasons and to distinguish between thorium and uranium in efforts to make a mixed actinide (U^{IV}/Th^{IV}) bimetallic system. However, all attempts to prepare such a U^{IV}/Th^{IV} complex through the reaction between mixtures of **6** and **7** and 1,4-dicyanobenzene yielded only the homo-bimetallic products **8** and **9**, as determined by NMR spectroscopy. The inability of this chemistry to produce the U^{IV}/Th^{IV} bimetallic system is not currently understood. In fact, similar efforts to prepare the monometallic complement of **8**, $[(C_5Me_4Et)_2U(Cl)\{\text{-}N{=}C(CH_3)\text{-}C_6H_4\text{-}C{\equiv}N\}]$, also yielded only the homo-bimetallic product **8**.

The molecular structures of **8** and **9** confirm that two $[(C_5Me_4Et)_2U(Cl)]$ or $[(C_5Me_5)_2Th(Br)]$ units are bridged by the 1,4-phenylenediketimide ligand to form a conjugated complex with an *anti* configuration, as shown in Figure 2. Both molecules reside on an inversion center, with U···U and Th···Th through-space distances of 10.956 Å and 11.049 Å, respectively. For the bimetallic complexes, each eight-coordinate metal center adopts a bent-metallocene geometry and contains a bridging ketimide and either a chloride (for **8**) or bromide (for **9**) ligand within the metallocene wedge. The actinide–halide bond lengths are consistent with reported values for other U–Cl (for **8**)[10] and Th–Br (for **9**)[12] complexes. Although the U(1)–N(1) bond length of 2.250(2) Å in **8** is slightly larger than the range (2.04(2)–2.225(5) Å) observed for previously reported U^{IV} ketimide complexes, the N(1)–C(21) bond length of 1.260(3) Å compares well to those reported for other U^{IV} ketimide structures.[8a,e,h] Similarly, for complex **9**, the Th(1)–N(1) bond length of 2.213(4) Å falls slightly short of the range (2.25(2)–2.286(5) Å) seen in other structurally characterized Th^{IV} ketimide complexes, but the N(1)–C(22) bond length of 1.266(6) Å is similar to that presented by the uranium system **8** and is in agreement with those reported for other Th^{IV} ketimide structures.[8a,e,f,g] Importantly, the π system providing the communication pathway between the two U^{IV} metal centers in **8** remains intact, as evidenced by the small torsion angles defined by N(1)–C(21)–C(23)–C(25) (7.3°) and C(22)–C(21)–C(23)–C(24) (8.3°). Similar metrical parameters are observed for the Th^{IV}/Th^{IV} bimetallic framework with N(1)–C(22)–C(24)–C(25) = 11.8° and C(23)–C(23)–C(24)-C(26) = 10.7°.

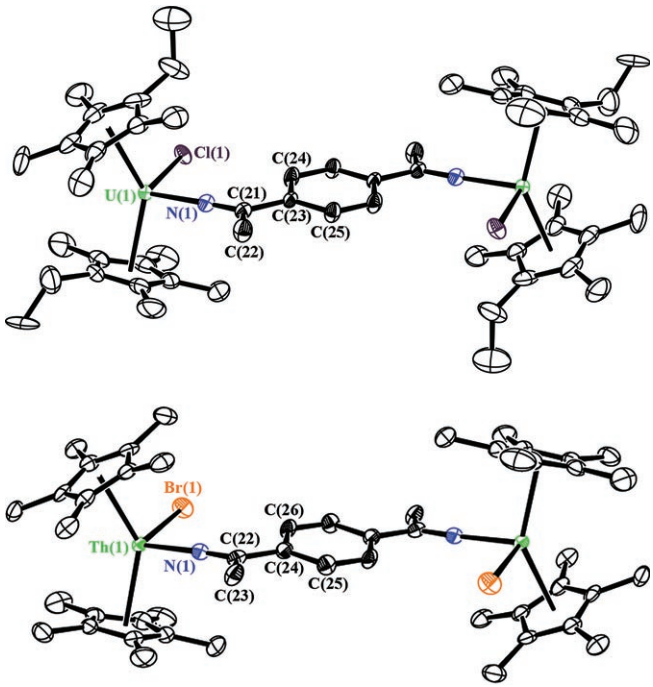

Figure 2. Molecular structures of **8** (top) and **9** (bottom) with thermal ellipsoids at the 50% probability level. Hydrogen atoms are omitted for clarity. The molecules reside on a crystallographic inversion center. Selected bond lengths [Å] and angles [°] for **8**: U(1)–N(1) 2.250(2), U(1)–Cl(1) 2.7106(13), N(1)–C(21) 1.260(3), N(1)–U(1)–Cl(1) 108.67(11), U(1)–N(1)–C(21) 175.29(19), U(1)–$C_5Me_4Et_{(cent)}$ 2.471(6), 2.493(6), $C_5Me_4Et_{(cent)}$–U(1)–$C_5Me_4Et_{(cent)}$ 140.2(2). Selected bond lengths [Å] and angles [°] for **9**: Th(1)–N(1) 2.213(4), Th(1)–Br(1) 2.8508(5), N(1)–C(22) 1.266(6), N(1)–Th(1)–Br(1) 100.69(10), Th(1)–N(1)–C(22) 176.2(3), Th(1)–$C_5Me_{5(cent)}$ 2.512(5), 2.525(5), $C_5Me_{5(cent)}$–Th(1)–$C_5Me_{5(cent)}$ 139.9(2).

Synthesis of monometallic ketimide complexes 10 and 11: Given the inability of this chemistry to produce a suitable mixed-actinide (U^{IV}/Th^{IV}) bimetallic system, the monometallic complexes $[(C_5Me_4Et)_2U\{\text{-}N{=}C(CH_3)\text{-}C_6H_4\text{-}C{=}N\}_2]$ (**10**) and $[(C_5Me_5)_2U(Cl)\{\text{-}N{=}C(CH_3)\text{-}(3,4,5\text{-}F_3\text{-}C_6H_2)\}]$ (**11**) were prepared to aid in the interpretation of the data obtained from the spectroscopic and magnetic studies on the U^{IV}/U^{IV} bimetallic complex (**8**). As shown in Scheme 1, the bis(ketimide) **10** was prepared by reaction of **4** with 1,4-dicyanobenzene (2 equiv). Following workup, complex **10** was isolated as a dark green solid in 45% isolated yield. Similarly, reaction of $[(C_5Me_5)_2U(CH_3)(Cl)]$ with 3,4,5-trifluorobenzonitrile (one equiv) affords the brick-red monometallic ketimide chloride derivative **11** in 18% yield [Eq. (1)]. Despite their low-to-moderate yields, both complexes were fully characterized, and their molecular structures are presented in Figure 3.

As with the bimetallic U^{IV}/U^{IV} complex **8**, both monometallic structures **10** and **11** feature an eight-coordinate U^{IV} metal center that adopts a bent-metallocene geometry and contains either two ketimide ligands (for **10**) or a ketimide and a chloride ligand (for **11**) within the metallocene wedge. The $U\text{–}N_{ketimide}$ (2.171(8), 2.187(8) Å for **10**; 2.155(5) Å for

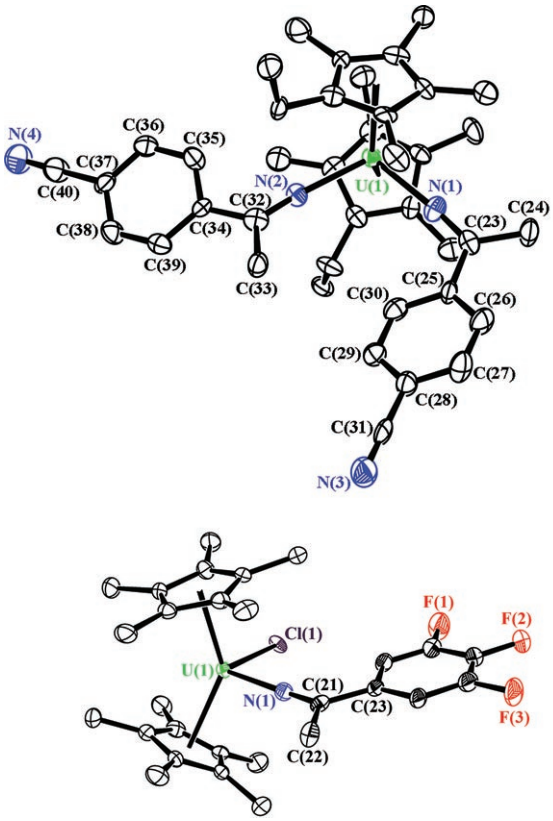

Figure 3. Molecular structures of **10** (top) and **11** (bottom) with thermal ellipsoids at the 50% probability level. Hydrogen atoms are omitted for clarity. Selected bond lengths [Å] and angles [°] for **10**: U(1)–N(1) 2.171(8), U(1)–N(2) 2.187(8), N(1)–C(23) 1.304(12), N(2)–C(32) 1.253(12), N(3)–C(31) 1.166(12), N(4)–C(40) 1.163(13), N(1)–U(1)–N(2) 106.0(3), U(1)–N(1)–C(23) 172.0(7), U(1)–N(2)–C(32) 174.0(8), U(1)–$C_5Me_4Et_{(cent)}$ 2.460(9), 2.459(9), $C_5Me_4Et_{(cent)}$–U(1)–$C_5Me_4Et_{(cent)}$ 141.8(3). Selected bond lengths [Å] and angles [°] for **11**: U(1)–N(1) 2.155(5), U(1)–Cl(1) 2.6649(13), N(1)–C(21) 1.263(7), N(1)–U(1)–Cl(1) 98.79(14), U(1)–N(1)–C(21) 176.9(4), U(1)–$C_5Me_{5(cent)}$ 2.447(6), 2.450(6), $C_5Me_{5(cent)}$–U(1)–$C_5Me_{5(cent)}$ 140.5(2).

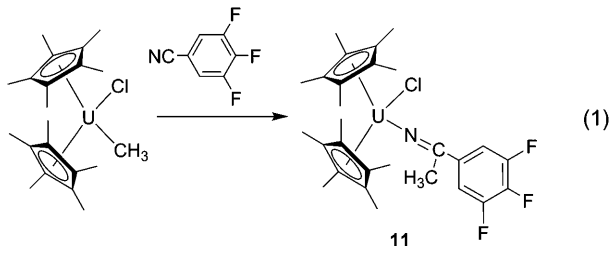

(1)

11) and N=C (1.304(12), 1.253(12) Å for **10**; 1.263(7) Å for **11**) bond lengths observed for the ketimide ligands in **10** and **11** are statistically consistent with reported values for other uranium ketimide complexes.[8a,e,h] The nitrile bond lengths (1.166(12), 1.163(13) Å) in complex **10** are as expected for uncoordinated nitrile groups.[13] The interplanar angles (φ) between the planes formed by ketimide atoms N=C(C_{Me})(C_{ipso}) and the ketimide aryl groups are 19.6 and 21.7°. These values compare well with those observed (φ = 5–35°) for other bis(ketimide)–Th/U complexes that do not possess *ortho* substituents on the ketimide aryl group.[8g,h]

Finally, it is noteworthy that the U–$N_{ketimide}$ and U–Cl bond lengths are substantially longer in the bimetallic U^{IV}/U^{IV} ketimide chloride complex **8** (U–N = 2.250(2) Å, U–Cl = 2.7106(13) Å) compared with the structurally related monometallic U^{IV} ketimide chloride complex **11** (U–N = 2.155(5) Å, U–Cl = 2.6649(13) Å).

Electrochemistry of 8 and 9: Metal–metal communication between the two $5f^2$ U^{IV} metals in **8** was assessed by using a combination of voltammetry, UV-visible/NIR absorption spectroscopy, and magnetic susceptibility. The electrochemical data provide the clearest manifestation of an interaction between the metal centers, as illustrated in Figure 4. Data for monometallic U^{IV} and Th^{IV} bis(ketimide) complexes all show the same general behavior illustrated for the known bis(ketimide) complexes, $[(C_5Me_5)_2An\{\text{-}N{=}CPh_2\}_2]$ (An = U (**12**), Th (**13**)).[8a,14] The oxidation wave (I) is attributed to a U^V/U^{IV} process, and the reduction wave (II) to a U^{IV}/U^{III} process. The more negative reduction wave (III) is attributed to a ketimide ligand-based process because it occurs at the same potential in both **12** and **13**, and no metal-based redox activity is expected for complexes of Th^{IV} under these experimental conditions.[15] The structurally related bimetallic thorium complex **9** exhibited two quasi-reversible reduction waves that also must be attributed to sequential one-electron reductions of the bridging ketimide ligand. Notably, the potentials of these waves are more positive than the re-

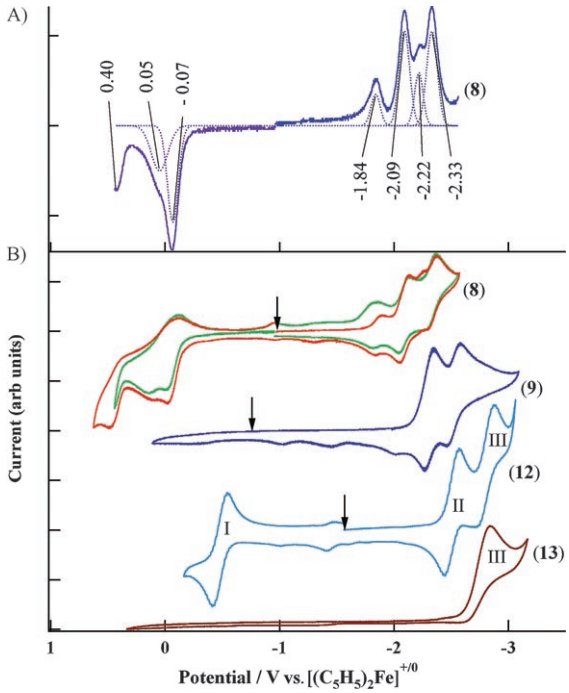

Figure 4. Voltammetric data in ≈0.1 M $[Bu_4N][B(fluoroaryl)_4]$/THF. A) Square-wave data for **8** with 10 mV pulse height at 60 Hz. B) Cyclic data for **8**, **9**, **12**,[14] and **13**[8a] at 200 mV s^{-1}. Rest potentials are indicated by vertical arrows.

duction wave of the terminal ketimide ligand in **12** and **13**, consistent with a more spatially delocalized redox orbital in the bridging ketimide.

The cyclic voltammogram for the bimetallic U^{IV}/U^{IV} system **8** is quite rich, and the inventory of redox processes is much more clearly discerned in the square-wave traces shown in Figure 4A. This complex clearly possesses four reduction waves clustered around −2 V and two poorly resolved oxidation waves centered at approximately 0 V (all potentials are versus $[(C_5H_5)_2Fe]^{+/0}$ in approximately 0.1 M $[Bu_4N][B(fluoroaryl)_4]$/THF, in which fluoroaryl = C_6F_5 or 3,5-$(CF_3)_2$-C_6H_3). The variations in the square-wave voltammetric peak heights in Figure 4A are not associated with differences in the number of electrons involved in the redox process, but rather reflect variations in the heterogeneous electron-transfer rate constants for the processes as described previously.[16] Based on the comparative behaviors illustrated in Figure 4, generic wave assignments follow in a straightforward manner. For the reduction waves, two must be attributable to bridging ligand-based processes, as seen for **9**, and the other two are ascribed to the one-electron reduction of each of the two U^{IV} centers. Similarly, the two oxidation waves at approximately 0 V are attributed to the one-electron oxidation of each of the two U^{IV} centers. The additional wave at around 0.4 V is ascribed to oxidation of the chloride ligand(s) and leads to some degradation of the reduction processes, as seen in the green trace (Figure 4B).

Specific assignments for each of the four reduction waves for **8** cannot be made solely on the basis of existing data. Based on the current amplitudes in the square-wave data, the processes at −1.84 and −2.22 V are comparable and exhibit less reversible behavior than the processes at −2.09 and −2.33 V. Inasmuch as the observed ligand-based reductions for **9** are also quasi-reversible in nature, it is plausible to suggest that these lower amplitude waves for **8** in the square-wave data are also ligand-based reductions. This would leave the waves at −2.09 and −2.33 V attributable to the U^{IV}/U^{III} processes. Clearly, however, these assignments remain equivocal.

For two equivalent but non-interacting redox centers, the theoretical separation between voltammetric waves associated with the same transformation (e.g., reduction or oxidation in the present case) is 36 mV. The observed separation of the two U^{IV}-based oxidation waves for **8** is 120 mV. If the reduction waves for **8** are assigned as suggested above, the two reduction waves corresponding to U^{IV}-based processes have a separation of 240 mV. The apparent difference in the separations for oxidation (120 mv) versus reduction (240 mV) waves must reflect, at least in part, the fact that the two reduction steps have an intervening ligand-based reduction process that would likely alter the redox potential of the second metal-based step. Regardless of the actual assignments of the reduction waves, the separations among these waves significantly exceed that for non-interacting centers. Thus, the electrochemical data illustrate a significant metal–metal interaction in **8**. For comparison, in bimetallic Mo^{V}/Mo^{V} systems containing an unsaturated bridging ligand and comparable metal–metal spacings, the separation between metal-based oxidation waves is 765 mV for [{Tp*(NO)(Cl)Mo}$_2${μ-(4,4′-bipyridine)}],[17] which contains a dipyridyl bridge and 340 mV for [{Tp*(O)(Cl)Mo}$_2${μ-(O-C_6H_4-CH=CH-C_6H_4-O)}] (Tp* = tris(3,5-dimethylpyrazol-1-yl)hydroborate),[18] which possesses a 1,4-diphenolate bridging ligand.

Electronic absorption spectroscopy of 8 and 11: The electronic absorption spectral data, even for isovalent bimetallic complexes such as **8** can, in principle, provide information about the extent of metal–metal interaction if suitable baseline data for monometallic species are available. We were unsuccessful in isolating the most appropriate monometallic analogue of **8** (e.g., $[(C_5Me_4Et)_2U(Cl)\{-N{=}C(CH_3)-C_6H_4-C{\equiv}N\}]$), but data are available for the monometallic chloroketimide with an electron-withdrawing phenyl group, $[(C_5Me_5)_2U(Cl)\{-N{=}C(CH_3)-(3,4,5-F_3-C_6H_2)\}]$ (**11**). Comparative UV-visible/NIR spectral data for **8** and **11** are presented in Figure 5. We focus on the f–f spectral region in the NIR where transitions derive from the $5f^2$ manifold of U^{IV}. The data for **11** are comparable to those previously reported by us for a wide range of U^{IV} bis(ketimide) complexes.[8] In particular, although these f–f transitions are parity-forbidden to a first approximation, we have attributed the substantial observed transition intensities to an intensity-stealing mechanism derived from energetically nearby, visible charge-transfer transitions involving the 5f orbitals.

The fidelity in the spectral band positions and relative intensities between **8** and **11** are quite remarkable, but there is a very surprising change in the spectral intensities. One might expect that the transition intensities for the bimetallic system would be approximately twice those for the structur-

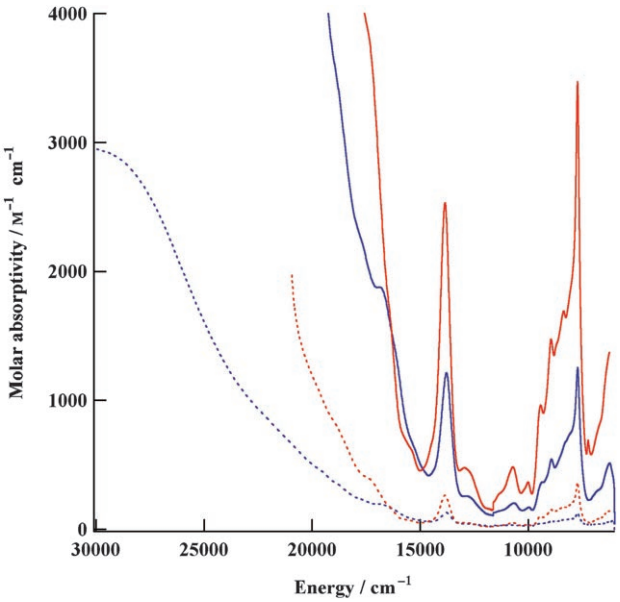

Figure 5. UV-visible (-----) and NIR (——, 10× the actual intensities) absorption spectral data for **8** (blue) and **11** (red) in toluene. Molar absorptivity values for **8** are per mole of complex.

ally analogous monometallic systems, since the absorption cross-section for the system with two chromophore metals should increase concomitantly. Here we see the rather surprising result that the transition intensities for these f–f bands actually decrease substantially for the bimetallic complex. The origin of this behavior is at present unclear.

Magnetic susceptibility of 8 and 10: Magnetic susceptibility and χT data for complexes **8** and **10** are shown in Figure 6. The high-temperature χT values for **8** (1.00 emu K mol^{-1} per U^{IV} ion) and **10** (0.81 emu K mol^{-1}) are consistent with reported values for U^{IV} ions in low-symmetry ligand fields.[2a,19]

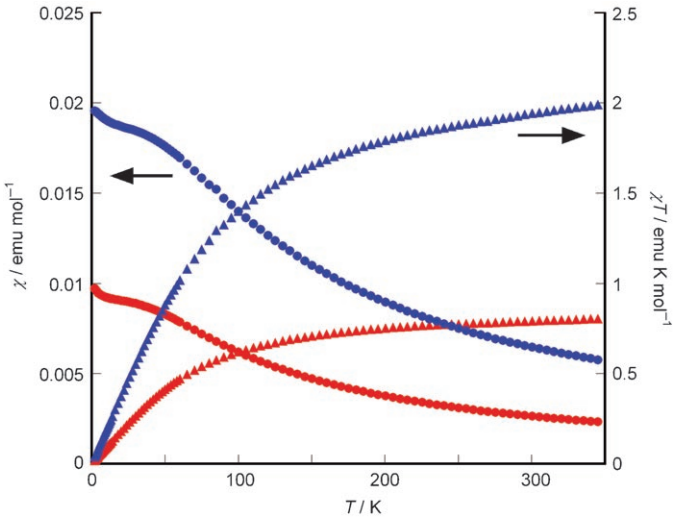

Figure 6. Magnetic data for **8** (blue) and **10** (red) from 2–350 K.

As expected for U^{IV} complexes, the primary temperature-dependent signature for these complexes is the ligand-field perturbation of the nominal $^3H_4$ ground state from the $5f^2$ configuration.[2a] This signature is clearly observed in the χT versus T data, which decreases over the whole temperature range and reaches around 0 emu K mol^{-1} at low temperature. This is also reflected by the χ versus T data that becomes temperature-independent at around 50 K for the complexes. Such behavior indicates orbital quenching of the $^3H_4$ term by the ligand field by removing the degeneracy of the nine ligand-field states to achieve an orbital singlet (nonmagnetic) ground state. Very small paramagnetic impurities, evident by the slight upturn (Curie tail) in the χ versus T data, are also exhibited by **8** and **10** at around 10 K (Figure 6).

In addition to the ligand-field effects for these ions, complex **8** has the potential to undergo additional perturbation of its magnetic susceptibility by magnetic coupling interactions between the ions. We have also shown that ketimide bridging ligands have the ability to promote magnetic communication between ions by means of other structural motifs,[8e] presumably as a result of the U^{IV}–N π-bonding interaction that involves the nitrogen lone pair. Previous studies have attempted to ascertain the presence of magnetic coupling in such systems through the use of structurally and magnetically similar complexes to reproduce and subtract ligand-field effects from the susceptibilities of multimetallic complexes. To perform a subtraction analysis to unambiguously detect magnetic coupling in complex **8**, a mixed-metal U^{IV}/Th^{IV} complex, which has not been synthetically forthcoming, is required to precisely reproduce the ligand-field effects in **8**. Another possible approach for the analysis of **8** could be to use twice the susceptibility of **10** in this fashion; however, the ligand-field energies of U^{IV} ketimide complexes have been shown to be very sensitive to substitution of the ketimide groups.[8h] As such, the results of such analysis for **8** using **10** are unreliable in this case.

Conclusion

Nitrile insertion chemistry with 1,4-dicyanobenzene was used to prepare simple dinuclear Th^{IV}/Th^{IV} and U^{IV}/U^{IV} complexes, thus enabling the study of the manifestations of electronic delocalization and magnetic interactions between actinide ions. Although the 1,4-phenylenediketimide bridging ligand possesses a significant covalent component to its bonding with uranium, evidence for magnetic superexchange is not evident by simple susceptibility measurements. However, the complex does display electronic communication between the metal centers through the π system of the dianionic bridging ligand, as judged by the substantial wave separation for the sequential reduction and oxidation processes of the two uranium metals. These results clearly show that these new bimetallic structures are useful platforms for studying metal–metal interactions and, with the prospect of preparing both mixed-valent and higher-nuclearity systems, offer new opportunities for exploring the electronic structure and valence delocalization in actinides.

Experimental Section

General synthetic procedures: Reactions and manipulations were performed in a recirculating Vacuum Atmospheres (Model HE-553-2 with a MO-40-2 Dri-Train or NEXUS with a 40CFM Dual Purifier NI-Train) dry box (N_2), or using standard Schlenk line techniques. Glassware was dried overnight at 150 °C before use. All NMR spectra were recorded in [D_8]toluene, [D_6]benzene, or [D_8]THF with a Bruker Avance 300 MHz spectrometer. Chemical shifts for ^1H and $^{13}C\{^1H\}$ NMR spectra were referenced to solvent impurities and ^{19}F NMR resonances were referenced to $CFCl_3$ at $\delta = 0.00$ ppm. Mass spectrometric (MS) analyses were obtained at the University of California, Berkeley Mass Spectrometry Facility with a VG ProSpec (EI) mass spectrometers. Elemental analyses were performed at the University of California, Berkeley Microanalytical Facility, on a Perkin–Elmer Series II 2400 CHNS analyzer.

Materials: Unless otherwise noted, reagents were purchased from commercial suppliers and used without further purification. Celite (Aldrich), alumina (Brockman I, Aldrich), and 4 Å molecular sieves (Aldrich) were dried under dynamic vacuum at 250 °C for 48 h prior to use. Anhydrous toluene (Aldrich), diethyl ether (Aldrich), tetrahydrofuran (Aldrich), dioxane (Aldrich), hexane (Aldrich), and pentane (Aldrich) were dried over KH for 24 h, passed through a column of activated alumina under

nitrogen and stored over activated 4 Å molecular sieves prior to use. [D_6]benzene (Aldrich, anhydrous), [D_8]THF (Cambridge Isotope Laboratories) and [D_8]toluene (Aldrich, anhydrous) were purified by storage over activated 4 Å molecular sieves under N_2 prior to use. [$(C_5Me_5)_2$Th-$(CH_3)_2$],[9] [$(C_5Me_5)_2U(CH_3)(Cl)$],[9] UCl_4,[20] [Bu_4N][$B(C_6F_5)_4$],[21] and [Bu_4N][$B(3,5\text{-}(CF_3)_2\text{-}C_6H_3)_4$][21] were prepared according to literature procedures.

Caution! *Depleted uranium (primarily isotope ^{238}U) and natural thorium (^{232}Th) are weak α emitters with a half-life of 4.47×10^9 years and 1.41×10^{10} years, respectively; manipulations and reactions should be carried out in monitored fume hoods or in an inert atmosphere dry box in a radiation laboratory equipped with α- and β-counting equipment.*

Synthesis of (C_5Me_4Et)MgCl·THF: In a dry box, a 1 L Schlenk flask equipped with a magnetic stirrer bar was charged with *i*PrMgCl (3.0 M/Et_2O, 112 mL, 224 mmol). The diethyl ether was removed from the solution under a dynamic vacuum to give a grey gelatinous mass that was suspended in toluene (250 mL). Ethyltetramethylcyclopentadiene (40.4 g, 269 mmol) was added to the suspension and the reaction vessel was sealed and removed from the dry box to a Schlenk line where it was placed under an argon atmosphere. The reaction mixture was heated to 105 °C for 12 h, then cooled to room temperature and returned to the dry box. The reaction was concentrated under reduced pressure and THF (100 mL) was added. Solvents were further removed to yield a thick white paste to which pentane (250 mL) was added. The resulting suspension was stirred at ambient temperature overnight. (C_5Me_4Et)MgCl·THF was collected as a white powder (58.4 g, 208 mmol, 93 %) by filtration over a medium-porosity fritted filter and was dried under a vacuum. ^{1}H NMR (300 MHz, [D_6]benzene, 25 °C): $\delta = 3.56$ (br s, 4H; α/β-C_4H_8O), 2.56 (q, ^3J(H,H) = 7.5 Hz, 2H; $C_5Me_4CH_2CH_3$), 2.16 (s, 6H; C_5Me_4Et), 2.12 (s, 6H; C_5Me_4Et), 1.30 (br s, 4H; α/β-C_4H_8O), 1.23 ppm (t, ^3J(H,H) = 7.5 Hz, 3H; $C_5Me_4CH_2CH_3$).

Synthesis of 3: In the dry box, a 250 mL Schlenk flask equipped with a stirrer bar was charged with UCl_4 (11.3 g, 29.7 mmol), (C_5Me_4Et)MgCl·THF (18.4 g, 65.3 mmol), and toluene (150 mL). On a Schlenk line, the reaction vessel was placed under nitrogen and heated at 105 °C for 24 h, after which the resulting maroon solution was filtered while hot over a Celite-padded coarse frit. The frit was washed with hot toluene until the washings were colorless. Solvents were removed under reduced pressure to give **3** as a dark red solid (17.5 g, 28.8 mmol, 97 %). Analytically pure samples of **3** were obtained by slow evaporation of a concentrated solution of **3** in toluene at room temperature. ^{1}H NMR (300 MHz, [D_6]benzene, 25 °C): $\delta = 22.99$ (s, 6H; $C_5Me_4CH_2CH_3$), 13.80 (s, 24H; C_5Me_4Et), −2.84 ppm (s, 4H; $C_5Me_4CH_2CH_3$); MS (70 eV): *m/z*: 606 $[M]^+$, 571 $[M-Cl]^+$, 457 $[M-C_5Me_4Et]^+$; elemental analysis calcd (%) for $C_{22}H_{34}Cl_2U$: C 43.50, H 5.64; found: C 43.18, H 5.51.

Synthesis of 4: [$(C_5Me_4Et)_2UCl_2$] (**3**, 8.0 g, 13 mmol), Et_2O (150 mL), and dioxane (10 mL) were added to a 250 mL Schlenk flask charged with a stirrer bar. Dropwise addition of MeMgBr (3.0 M/Et_2O, 13.2 mL, 4.40 mmol) resulted in the immediate formation of a white precipitate. The mixture was stirred at room temperature for 16 h. The solvent was removed under reduced pressure to give a red solid, which was redissolved in hexane (30 mL) and filtered through a Celite-padded coarse frit. The frit was washed with hexane until the filtrate was colorless. The red-orange filtrate was concentrated (20 mL) and cooled at −35 °C to form dark red crystalline **4** (5.3 g, 9.4 mmol, 72 %). ^{1}H NMR (300 MHz, [D_8]THF, 25 °C): $\delta = 14.5$ (s, 6H; $C_5Me_4CH_2CH_3$), 5.6 (s, 12H; C_5Me_4Et), 5.1 (s, 12H; C_5Me_4Et), −4.3 (s, 4H; $C_5Me_4CH_2CH_3$), −137.2 ppm (s, 6H; U-CH_3); MS (70 eV): *m/z*: 566 $[M]^+$, 551 $[M-CH_3]^+$, 536 $[M-2CH_3]^+$; elemental analysis calcd (%) for $C_{31}H_{48}U$: C 56.52, H 7.34; found: C 56.79, H 7.89.

Synthesis of 6: Complex **6** was prepared in situ as needed for the synthesis of **8** using the following procedure: A solution of Ph_3CCl (0.52 g, 1.9 mmol) in THF (15 mL) was added to a 125 mL side-arm flask charged with **4** (1.1 g, 1.9 mmol) and THF (10 mL). The mixture was stirred at room temperature for 16 h to give **6** as a red solution. ^{1}H NMR (300 MHz, [D_6]benzene, 22 °C): $\delta = 9.37$ (s, 24H; C_5Me_4Et), 6.04 (s, 6H; $C_5Me_4CH_2CH_3$), 4.53 (s, 4H; $C_5Me_4CH_2CH_3$), −166.78 ppm (s, 3H; U-CH_3).

Synthesis of 7: Complex **7** was prepared in situ as needed for the synthesis of **9** according to the following procedure: A 125 mL side-arm flask was charged with **5** (0.45 g, 0.84 mmol) and toluene (20 mL). A solution of Ph_3CBr (0.28 g, 0.86 mmol) in toluene (10 mL) was added to this clear, pale off-white solution of **5** resulting in an immediate color change to yellow. The mixture was stirred at room temperature for 16 h to give **7** as a yellow solution. The ^{1}H NMR spectrum of **7** is identical to that reported for [$(C_5Me_5)_2Th(CH_3)(Cl)$].[9] ^{1}H NMR (300 MHz, [D_6]benzene, 25 °C): $\delta = 1.97$ (s, 30H; C_5Me_5), 0.30 ppm (s, 3H; Th-CH_3).

Synthesis of 8: A solution of Ph_3CCl (0.52 g, 1.9 mmol) in THF (15 mL) was added to a 125 mL side-arm flask charged with **4** (1.1 g, 1.9 mmol) and THF (10 mL). The mixture was stirred at ambient temperature for 16 h to give **6** as a red solution. Next, a solution of 1,4-dicyanobenzene (0.12 g, 0.94 mmol) in THF (15 mL) was added to the solution of **6**, resulting in a dark brown solution, which was stirred at room temperature for 16 h. The volatile compounds were removed under reduced pressure to afford a brown powder, which was redissolved in pentane (≈25 mL) and filtered through a Celite-padded coarse porosity frit. The frit was washed with pentane until the washings were colorless. The brown filtrate was concentrated (20 mL) and cooled to −35 °C to afford dark brown crystalline **8** (0.54 g, 0.41 mmol, 43 %). ^{1}H NMR (300 MHz, [D_6]benzene, 25 °C): $\delta = 4.3$ (s, 12H; C_5Me_4Et), 2.7 (s, 12H; C_5Me_4Et), 2.3 (s, 12H; C_5Me_4Et), 2.0 (s, 20H; C_5Me_4Et (12H) and C_5Me_4Et (8H)), 1.7 (s, 12H; C_5Me_4Et), −0.55 (s, 4H; Ar-*H*), −0.90 (s, 3H; N=C(*Me*)), −39.5 ppm (s, 3H; N=C(*Me*)); elemental analysis calcd (%) for $C_{54}H_{78}Cl_2N_2U_2$: C 49.81, H 6.04, N 2.15; found: C 49.68, H 6.10, N 2.17.

Synthesis of 9: A 125 mL side-arm flask was charged with **5** (0.45 g, 0.84 mmol) and toluene (10 mL). A solution of Ph_3CBr (0.28 g, 0.86 mmol) in toluene (10 mL) was added dropwise to the clear, pale off-white thorium solution of **5**, resulting in an immediate color change to yellow. The mixture was stirred at room temperature for 16 h to give **7** as a yellow solution. Next, a solution of 1,4-dicyanobenzene (0.054 g, 0.42 mmol) in toluene (10 mL) was added dropwise with stirring to the solution of **7**, resulting in a bright orange solution, which was stirred at room temperature for 4 h, filtered through a Celite-padded coarse porosity frit, and the volatile compounds removed under reduced pressure. Two successive recrystallizations from a solution of THF (5 drops) and diethyl ether (5 mL) at −30 °C produced orange crystalline **9** (0.078 g, 0.059 mmol, 14 %). ^{1}H NMR (300 MHz, [D_6]benzene, 25 °C): $\delta = 8.10$ (s, 4H; Ar-*H*), 2.22 (s, 6H; N=C(*Me*)), 2.04 (s, 60H; C_5Me_5); elemental analysis calcd (%) for $C_{50}H_{70}Br_2N_2Th_2$: C 45.39, H 5.33, N 2.12; found: C 45.39, H 5.26, N 2.25.

Synthesis of 10: A solution of **4** (1.0 g, 1.8 mmol) in THF (20 mL) was added dropwise to a 125 mL side-arm flask charged with 1,4-dicyanobenzene (0.47 g, 3.7 mmol) and THF (20 mL), resulting in a dark green solution that was stirred at room temperature for 1 h. The volatile compounds were removed under reduced pressure to give a green powder, which was redissolved in toluene (20 mL) and filtered through a Celite-padded coarse frit. The frit was washed with toluene until the washings were colorless. The green filtrate was concentrated (≈10 mL), layered with hexane (≈10 mL), and cooled to −35 °C to give dark green crystalline, analytically pure **10** (0.37 g, 0.45 mmol, 25 %). ^{1}H NMR (300 MHz, [D_8]toluene, 65 °C): $\delta = 20.5$ (s, 4H; Ar-*H*), 2.3 (s, 4H; C_5Me_4Et), −1.0 (s, 12H; C_5Me_4Et), −1.7 (s, 12H; C_5Me_4Et), −4.6 (s, 6H; C_5Me_4Et), −10.6 ppm (s, 6H; N=C(*Me*)); elemental analysis calcd (%) for $C_{40}H_{48}N_4U$: C 58.38, H 5.88, N 6.81; found: C 58.09, H 5.98, N 6.61.

Synthesis of 11: A solution of 3,4,5-trifluorobenzonitrile (0.31 g, 1.92 mmol, 2.3 equiv) in 1:1 (v/v) pentane/toluene (20 mL) was added dropwise to a 250 mL side-arm flask charged with [$(C_5Me_5)_2U(CH_3)(Cl)$] (0.47 g, 0.84 mmol) and pentane (100 mL), during which time the solution changed color from orange-red to dark orange-brown. The reaction mixture was stirred at room temperature for 14 h. The volatile compounds were removed under reduced pressure to give a brown solid, which was extracted with pentane (10 mL). The resulting suspension was filtered through a Celite-padded coarse frit. The filtered solid was washed with warm pentane (3×5 mL). The combined filtrates were cooled to −30 °C to give brick-red crystalline, analytically pure **11** (0.11 g, 0.15 mmol, 18 %). X-ray quality crystals of **11** were obtained by slow evaporation of

a concentrated solution of **11** in hexane at room temperature. (300 MHz, [D_6]benzene, 25 °C): $\delta = 7.84$ (s, 3H; CH_3), 3.89 (s, 30H; C_5Me_5), −2.81 ppm (s, 2H; *ortho*-$C_6H_2F_3$); ^{19}F NMR (300 MHz, [D_6]benzene, 25 °C, $CFCl_3$): $\delta = -64.85$ (s, 1 F; *para*-$C_6H_2F_3$), −129.15 ppm (s, 2 F; *meta*-$C_6H_2F_3$); MS (70 eV): *m*/*z*: 715.4 $[M]^+$; elemental analysis calcd (%) for $C_{36}H_{40}N_2F_6U$: C 46.97, H 4.93, N 1.96; found: C 47.06, H 5.10, N 1.78.

Electronic absorption spectroscopy: Electronic absorption spectral data were obtained for solutions of complexes **8** and **11** in toluene over the wavelength range 280–2500 nm on a Perkin–Elmer Model Lambda 950 UV-visible/NIR spectrophotometer. Data were collected in 1 mm or 1 cm path-length cuvettes loaded in the Vacuum Atmospheres dry box systems described above. Samples were typically run at multiple dilutions to optimize absorbance in the UV-visible and NIR, respectively. Spectral resolution was typically 2 nm in the visible region and 4–6 nm in the NIR.

Electrochemistry: Cyclic wave voltammetric data were obtained in the Vacuum Atmospheres dry box systems described above. All data were collected with a Perkin–Elmer Princeton Applied Research Corporation (PARC) Model 263 potentiostat under computer control with PARC Model 270 software. All sample solutions contained about 2–3 mM complex with 0.1 M $[Bu_4N][B(C_6F_5)_4]$ or $[Bu_4N][B(3,5\text{-}(CF_3)_2\text{-}C_6H_3)_4]$ supporting electrolyte in THF. All data were collected with the positive-feedback IR compensation feature of the software/potentiostat activated to ensure minimal contribution to the voltammetric waves from uncompensated solution resistance (typically ≈ 1 kΩ under the conditions employed). Solutions were contained in PARC Model K0264 microcells consisting of a ≈ 3 mm diameter Pt disk working electrode, a Pt wire counter electrode, and an Ag wire quasi-reference electrode. Scanning rates from 20 to 5000 mV s^{-1} were employed in the cyclic voltammetry scans to assess the chemical and electrochemical reversibility of the observed redox transformations. Half-wave potentials were determined from the peak values in the square-wave voltammograms or from the average of the cathodic and anodic peak potentials in the reversible cyclic voltammograms. Potential calibrations were performed at the end of each data collection cycle using the ferrocenium/ferrocene couple as an internal standard. Electronic absorption and cyclic voltammetric data were analyzed with Wavemetrics IGOR Pro (Version 4.0) software on a Macintosh platform.

Magnetic susceptibility: Magnetic susceptibility data were collected with a Quantum Design Superconducting Quantum Interference Device (SQUID) magnetometer at 5 T from 2 to 350 K. The samples were pulverized and sealed in a 5 mm Wilmad 505-PS NMR tube along with a small amount of quartz wool that held the sample near the center of the tube. Contributions to the magnetization from the quartz wool and the NMR tube were measured independently and subtracted from the total measured signal. Diamagnetic corrections were made with the use of Pascal's constants.

Crystallographic experimental details: Crystals were mounted in a nylon cryoloop using Paratone-N oil under an argon gas flow. The data were collected on a Bruker D8 APEX II charge-coupled-device (CCD) diffractometer, with a KRYO-FLEX liquid nitrogen vapor-cooling device. The instrument was equipped with a graphite-monochromatized $Mo_{K\alpha}$ X-ray source ($\lambda = 0.71073$ Å), with MonoCap X-ray source optics. Hemispheres of data were collected with ω scans. Data collection and initial indexing and cell refinement were handled with APEX II software.[22] Frame integration, including Lorentz-polarization corrections, and final cell parameter calculations were carried out with SAINT+ software.[23] The data were corrected for absorption with the SADABS program.[24] Decay of reflection intensity was monitored by analysis of redundant frames. The structure was solved with direct methods and difference Fourier techniques. Unless otherwise noted, non-hydrogen atoms were refined anisotropically and hydrogen atoms were treated as idealized contributions. Residual electron density originating from solvent contributions was removed with SQUEEZE/PLATON.[25] Structure solution, refinement, graphics, and creation of publication materials were performed with SHELXTL.[26] Additional details of data collection and structure refinement are listed in Table 1. CCDC-681147 (**3**), 681148 (**4**), 681149 (**8**·2THF), 681150 (**9**·2THF), 681151 (**10**·0.5C_7H_8), and 681152 (**11**) contain the supplementary crystallographic data for this paper. These data can be obtained free of charge from The Cambridge Crystallographic Data Centre via www.ccdc.cam.ac.uk/data_request/cif.

Acknowledgements

For financial support of the work, we acknowledge Los Alamos National Laboratory (Frederick Reines PD Fellowship to E.J.S. & Director's PD Fellowship to E.J.S., C.R.G. and J.A.P.D.T), the LANL G. T. Seaborg Institute (PD Fellowships to E.J.S. and C.R.G.), the LANL Laboratory Directed Research & Development program, and the Division of Chemical Sciences, Office of Basic Energy Sciences, Heavy Element Chemistry program. Jim Cruz (Los Alamos National Laboratory) is acknowledged for the cover picture artwork.

[1] a) K. P. Mörtl, J.-P. Sutter, S. Golhen, L. Ouahab, O. Kahn, *Inorg. Chem.* **2000**, *39*, 1626–1627; b) R. Patschke, J. D. Breshears, P. Brazis, C. R. Kannewurf, S. J. L. Billinge, M. G. Kanatzidis, *J. Am. Chem. Soc.* **2001**, *123*, 4755–4762; c) N. J. Curro, T. Caldwell, E. D.

Table 1. Crystallographic experimental parameters for **3**, **4**, and **8**–**11**.

	3	**4**	**8**·2THF	**9**·2THF	**10**·0.5C_7H_8	**11**
empirical formula	$C_{22}H_{34}Cl_2U$	$C_{28}H_{40}U$	$C_{46}H_{94}Cl_2N_2O_2U_2$	$C_{58}H_{86}Br_2N_2O_2Th_2$	$C_{43.5}H_{52}N_4U$	$C_{28}H_{35}ClF_3N$
formula weight	607.42	614.63	1254.19	1467.19	868.92	716.05
crystal system	monoclinic	monoclinic	monoclinic	monoclinic	monoclinic	monoclinic
a [Å]	8.0517(5)	8.4801(6)	10.6609(9)	10.5548(7)	21.665(6)	9.0965(6)
b [Å]	18.5974(11)	14.3568(10)	15.4993(13)	15.4869(10)	10.062(3)	26.4129(17)
c [Å]	8.4043(5)	18.8531(14)	17.5406(14)	17.8994(12)	17.972(5)	11.4820(7)
β [°]	118.2980(10)	100.798(1)	97.3740(10)	97.4850(10)	95.077(4)	101.2530(10)
V [Å^3]	1108.07(12)	2254.7(3)	2874.4(4)	2900.9(3)	3902.3(19)	2705.7(3)
space group	$P2_1/m$	$P2_1/c$	$P2_1/c$	$P2_1/c$	$P2_1/c$	$P2_1/n$
Z	2	4	2	2	4	4
ρ [g cm^{-3}]	1.821	1.811	1.449	1.680	1.479	1.758
$\mu(Mo_{K\alpha})$ [mm^{-1}]	7.568	7.211	5.751	6.538	4.194	6.135
T [K]	120(1)	120(1)	120(1)	141(1)	141(1)	141(1)
$2\theta_{max}$ [°]	57.86	56.24	56.36	57.82	50.24	54.88
min/max transmission	0.5182/0.8048	0.3568/0.3916	0.4597/0.8026	0.3029/0.6951	0.4876/0.8502	0.2984/0.7914
total reflns	9749	18552	31121	31905	35581	29398
unique reflns	2239	5096	6674	7124	6909	6150
parameters	118	238	289	298	418	307
R_1(wR_2) (all data)	0.0521(0.1490)	0.0336(0.0615)	0.0533(0.1275)	0.0540(0.0857)	0.0976(0.1446)	0.0560(0.1051)

Bauer, L. A. Morales, M. J. Graf, Y. Bang, A. V. Balatsky, J. D. Thompson, J. L. Sarrao, *Nature* **2005**, *434*, 622–625; d) H. D. Selby, B. C. Chan, R. F. Hess, K. D. Abney, P. K. Dorhout, *Inorg. Chem.* **2005**, *44*, 6463–6469; e) D. L. Clark, S. S. Hecker, G. D. Jarvinen, M. P. Neu in *The Chemistry of the Actinide and Transactinide Elements, Vol. 2* (Eds: L. R. Morss, N. M. Edelstein, J. Fuger), Springer, Dordrecht, **2006**, pp. 813–1264; f) E. J. Schelter, D. E. Morris, B. L. Scott, J. D. Thompson, J. L. Kiplinger, *Inorg. Chem.* **2007**, *46*, 5528–5536.

[2] a) E. A. Boudreaux, L. N. Mulay, *Theory and Applications of Molecular Paramagnetism*, Wiley, New York, **1976**; b) R. L. Carlin, *Magnetochemistry*, Springer, Berlin, **1986**; c) O. Kahn, *Molecular Magnetism*, Wiley-VCH, New York, **1993**.

[3] For examples, see: a) L. M. Mokry, N. S. Norman, C. J. Carrano, *Angew. Chem.* **1996**, *108*, 1676–1677; *Angew. Chem. Int. Ed. Engl.* **1996**, *35*, 1497–1498; b) P. B. Duval, C. J. Burns, D. L. Clark, D. E. Morris, B. L. Scott, J. D. Thompson, E. L. Werkema, L. Jia, R. A. Andersen, *Angew. Chem.* **2001**, *113*, 3461–3465; *Angew. Chem. Int. Ed.* **2001**, *40*, 3357–3361; c) L. Salmon, P. Thuéry, M. Ephritikhine, *Polyhedron* **2004**, *23*, 623–627; d) J. C. Berthet, P. Thuéry, M. Ephritikhine, *Chem. Commun.* **2005**, 3415–3417; e) M. Ephritikhine, *Dalton Trans.* **2006**, 2501–2516, and references therein; f) G. Nocton, F. Burdet, J. Pecaut, M. Mazzanti, *Angew. Chem.* **2007**, *119*, 7718–7722; *Angew. Chem. Int. Ed.* **2007**, *46*, 7574–7578, and references therein.

[4] For self-assembled actinide supramolecules, see: a) P. Thuéry, B. Masci, *Supramol. Chem.* **2003**, *15*, 95–99; b) P. Thuéry, C. Villiers, J. Jaud, M. Ephritikhine, B. Masci, *J. Am. Chem. Soc.* **2004**, *126*, 6838–6839; c) W. J. Evans, S. A. Kozimor, J. W. Ziller, *Science* **2005**, *309*, 1835–1838; d) J. L. Kiplinger, J. A. Pool, E. J. Schelter, J. D. Thompson, B. L. Scott, D. E. Morris, *Angew. Chem.* **2006**, *118*, 2090–2095; *Angew. Chem. Int. Ed.* **2006**, *45*, 2036–2041.

[5] a) T. Le Borgne, E. Rivière, J. Marrot, P. Thuéry, J. J. Girerd, M. Ephritikhine, *Chem. Eur. J.* **2002**, *8*, 773–783; b) L. Salmon, P. Thuéry, E. Rivière, J. J. Girerd, M. Ephritikhine, *Chem. Commun.* **2003**, 762–763; c) L. Salmon, P. Thuéry, E. Rivière, J. J. Girerd, M. Ephritikhine, *Dalton Trans.* **2003**, 2872–2880; d) L. Salmon, P. Thuéry, E. Rivière, M. Ephritikhine, *Inorg. Chem.* **2006**, *45*, 83–93; e) S. A. Kozimor, B. M. Bartlett, J. D. Rinehart, J. R. Long, *J. Am. Chem. Soc.* **2007**, *129*, 10672–10674.

[6] R. K. Rosen, R. A. Andersen, N. M. Edelstein, *J. Am. Chem. Soc.* **1990**, *112*, 4588–4590.

[7] E. J. Schelter, R. Wu, B. L. Scott, J .D. Thompson, D. E. Morris, J. L. Kiplinger, *Angew. Chem.* **2008**, *120*, 3035–3038; *Angew. Chem. Int. Ed.* **2008**, *47*, 2993–2996.

[8] a) K. C. Jantunen, C. J. Burns, I. Castro-Rodriguez, R. E. Da Re, J. T. Golden, D. E. Morris, B. L. Scott, F. L. Taw, J. L. Kiplinger, *Organometallics* **2004**, *23*, 4682–4692; b) D. E. Morris, R. E. Da Re, K. C. Jantunen, I. Castro-Rodriguez, J. L. Kiplinger, *Organometallics* **2004**, *23*, 5142–5153; c) R. E. Da Re, K. C. Jantunen, J. T. Golden, J. L. Kiplinger, D. E. Morris, *J. Am. Chem. Soc.* **2005**, *127*, 682–689; d) A. E. Clark, R. L. Martin, P. J. Hay, J. C. Green, K. C. Jantunen, J. L. Kiplinger, *J. Phys. Chem. A* **2005**, *109*, 5481–5491; e) E. J. Schelter, J. M. Veauthier, J. D. Thompson, B. L. Scott, K. D. John, D. E. Morris, J. L. Kiplinger, *J. Am. Chem. Soc.* **2006**, *128*, 2198–2199; f) E. J. Schelter, D. E. Morris, B. L. Scott, J. L. Kiplinger, *Chem. Commun.* **2007**, 1029–1031; g) E. J. Schelter, P. Yang, B. L. Scott, R. E. Da Re, K. C. Jantunen, R. L. Martin, P. J. Hay, D. E. Morris, J. L. Kiplinger, *J. Am. Chem. Soc.* **2007**, *129*, 5139–5152; h) E. J. Schelter, P. Yang, B. L. Scott, J. D. Thompson, R. L. Martin, P. J. Hay, D. E. Morris, J. L. Kiplinger, *Inorg. Chem.* **2007**, *46*, 7477–7488.

[9] These syntheses are similar to those reported for $(C_5Me_5)MgCl\cdot(THF)$, $[(C_5Me_5)_2UCl_2]$, and $[(C_5Me_5)_2U(CH_3)_2]$: P. J. Fagan, J. M. Manriquez, E. A. Maatta, A. M. Seyam, T. J. Marks, *J. Am. Chem. Soc.* **1981**, *103*, 6650–6667.

[10] R. G. Peters, B. L. Scott, C. J. Burns, *Acta Cryst. Sect. C: Cryst. Struct. Commun.* **1999**, *55*, 1482–1483, and references therein.

[11] Trityl compounds have been previously used as methide abstraction reagents; for relevant examples, see: a) J. L. Kiplinger, K. D. John, D. E. Morris, B. L. Scott, C. J. Burns, *Organometallics* **2002**, *21*, 4306–4308; b) E. J. Hawrelak, P. A. Deck, *Organometallics* **2004**, *23*, 9–11.

[12] D. L. Rabinovich, G. L. Schimek, W. T. Pennington, J. B. Nelson, K. D. Abney, *Acta Cryst. Sect. C: Cryst. Struct. Commun.* **1997**, *53*, 1794–1797, and references therein.

[13] F. H. Allen, O. Kennard, D. G. Watson, L. Bremmer, A. G. Orpen, R. Taylor, *J. Chem. Soc. Perkin Trans. 2* **1987**, S1–S19.

[14] J. L. Kiplinger, D. E. Morris, B. L. Scott, C. J. Burns, *Organometallics* **2002**, *21*, 3073–3075.

[15] M. S. Wickleder, B. Fourest, P. K. Dorhout in *The Chemistry of the Actinide and Transactinide Elements, Vol. 1* (Eds: L. R. Morss, N. M. Edelstein, J. Fuger) Springer, Dordrecht , **2006**, pp. 52–160.

[16] a) J. J. O'Dea, J. Osteryoung, R. A. Osteryoung, *Anal. Chem.* **1981**, *53*, 695–701; b) M. J. Nuwer, J. J. O'Dea, J. Osteryoung, *Anal. Chim. Acta* **1991**, *251*, 13–25.

[17] A. M. W. Cargill Thompson, D. Gatteschi, J. A. McCleverty, J. A. Navas, E. Rentschler, M. D. Ward, *Inorg. Chem.* **1996**, *35*, 2701–2703.

[18] S. R. Bayly, E. R. Humphrey, H. de Chair, C. G. Paredes, Z. R. Bell, J. C. Jeffery, J. A. McCleverty, M. D. Ward, F. Totti, D. Gatteschi, S. Courric, B. R. Steele, C. G. Screttas, *J. Chem. Soc. Dalton Trans.* **2001**, 1401–1414.

[19] a) L. Salmon, P. Thuery, E. Riviere, S, Miyamoto, T. Yamato, M. Ephritikhine, *New J. Chem.* **2006**, *30*, 1220–1227; b) I. Castro-Rodriguez, K. Meyer, *Chem. Commun.* **2006**, 1353–1368.

[20] J. L. Kiplinger, D. E. Morris, B. L. Scott, C. J. Burns, *Organometallics* **2002**, *21*, 5978–5982.

[21] a) R. J. LeSuer, W. E. Geiger, *Angew. Chem.* **2000**, *112*, 254–256; *Angew. Chem. Int. Ed.* **2000**, *39*, 248–250; b) R. J. LeSuer, C. Buttolph, W. E. Geiger, *Anal. Chem.* **2004**, *76*, 6395–6401; c) F. Barrière, R. J. LeSuer, W. E. Geiger in *Trends in Molecular Electrochemistry* (Eds: A. J. L. Pombeiro, C. Amatore), Marcel Dekker Inc., New York, **2004**, pp. 413–444; d) A. Nafady, P. J. Costa, M. J. Calhorda, W. E. Geiger, *J. Am. Chem. Soc.* **2006**, *128*, 16587–16599.

[22] APEX II, Data Collection Software, Version 1.08, Bruker Analytical X-ray Instruments, Inc., Madison, WI 53719, **2004**.

[23] SAINT+, Data Collection Software Version 7.06, Bruker Analytical X-ray Instruments, Inc., Madison, WI 53719, **2003**.

[24] G. M. Sheldrick, SADABS, Empirical Absorption Corrective Program, Version 2.03, University of Göttingen, Göttingen (Germany), **2001**.

[25] A. L. Spek, *Acta Cryst.* **1990**, *A46*, C34.

[26] SHELXTL, Version 5.10, Bruker Analytical X-ray Instruments, Inc. Madison, WI 53719, **1997**.

Received: March 31, 2008
Revised: June 17, 2008
Published online: August 7, 2008

